ACS APPLIED NANO MATERIALS

www.acsanm.org Article

High Harmonic Generation from Laser-Induced Plasmas of Ni-Doped $CsPbBr_3$ Nanocrystals: Implications for Extreme Ultraviolet Light Sources

Srinivasa Rao Konda,* Venugopal Rao Soma, Murali Banavoth, Ravi Ketavath, Venkatesh Mottamchetty, Yu Hang Lai, and Wei Li*

Cite This: *ACS Appl. Nano Mater.* 2021, 4, 8292−8301 Read Online

ACCESS | Metrics & More | Article Recommendations

ABSTRACT: The development of versatile two-dimensional (2D) nanocrystals (NCs), with superior nonlinear optical (NLO) properties, is essential for various applications in photonics and optical communications. In this work, we demonstrate efficient high-order harmonic generation (HHG) from the laser-induced plasmas (LIPs) of $CsPbBr_3$ and Ni-doped $CsPbBr_3$ NCs. The present study has been directed at unraveling the role of dopants in the emission of intense harmonics from the LIP of purposefully engineered $CsPbBr_3$ colloidal NCs. The trend observed in the harmonic yield enhancement is found to be similar to the increase in their third-order NLO properties [nonlinear refractive index (n_2), nonlinear optical susceptibility ($\chi^{(3)}$)] of the same NCs studied at a wavelength of 800 nm. Ni-doped $CsPbBr_3$ NCs containing plasma spreading allowed optimization of the delay between nanosecond (ns) heating pulse and driving pulse (single-color pump) for an enhancement in the conversion efficiency of harmonics. We believe that the emission of harmonics from the LIPs of these pristine, Ni-doped $CsPbBr_3$ colloidal 2D NCs reported here provides the means to address the increase in the efficiency of extreme ultraviolet radiation, useful in attosecond spectroscopic studies.

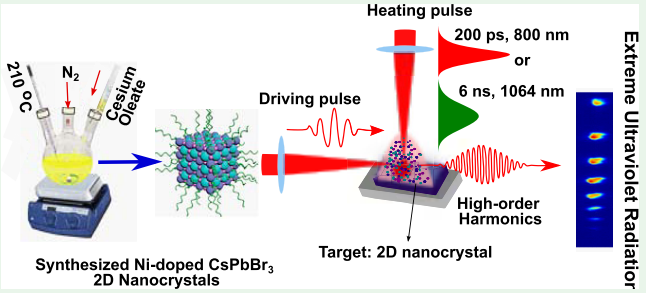

KEYWORDS: *HHG, $CsPbBr_3$, Ni-doped $CsPbBr_3$, 2D nanocrystals, perovskites, plasma plumes*

1. INTRODUCTION

Organic−inorganic lead halide perovskite nanocrystals (NCs) have ignited extensive research awareness over the past decade due to their exciting physical, optical, and optoelectronic properties. Perovskite colloidal semiconductor NCs are an evolving class of nonlinear optical (NLO) materials owing to their remarkable optical/optoelectronic properties and potential in applications such as lasers, light-emitting diodes, photodetectors, and photodiodes.[1−8] Beyond the above-mentioned applications, the attention in exploration related to the NLO applications has also been acquisitive. This is due to the fact that a strong saturable absorption behavior is mandatory for developing mode-locked lasers and superior multiphoton absorption cross sections are required for two-photon pumped lasing, bio-imaging, etc., and several materials have been studied in both bulk and nanostructured forms.[9−11] The (a) synthesis, (b) NLO properties (at 800 nm), and (c) excited-state dynamics (at 400 nm) of pristine, Ni-doped $CsPbBr_3$ colloidal two-dimensional (2D) NCs were explored in our earlier work.[12] Ni-doped $CsPbBr_3$ possessed strong two-photon absorption (2PA) coefficients (due to the strong coupling between the plasmons and excitons within the NCs), with an enhanced 2PA cross section (due to the charge transfer induced by localized surface plasmons) and third-order nonlinear optical susceptibility compared to pristine $CsPbBr_3$. Likewise, these halide perovskites hold stirring assets such as high carrier mobility and tunable photoluminescence.[13−16]

High harmonic generation (HHG) has been extensively investigated in the areas of extreme NLO interactions between solids, gas, and plasma plumes.[17−25] The HHG process attracted the attention of researchers from the perspective of application in improvement of light sources in the extreme ultraviolet (EUV/XUV) spectral regime and attosecond photonics.[26−32] Earlier works demonstrated an enhanced harmonic yield from the plasma plumes of different bulk materials, nanoparticles, and quantum dots.[33−36] Recently, HHG from hybrid organic−inorganic perovskite (with a

Received: June 7, 2021
Accepted: July 21, 2021
Published: August 3, 2021

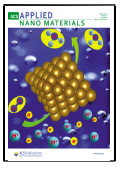

https://doi.org/10.1021/acsanm.1c01490
ACS Appl. Nano Mater. 2021, 4, 8292−8301

general form of $MAPbX_3$, where MA = $CH_3NH_3^+$ and X = I, Br, and Cl) thin films exciting them with strong mid-infrared laser pulses and with linear, elliptical polarization was reported.[37,38] However, in this work, we focused on generating extreme ultraviolet radiation (10−100 nm range) from plasma plumes of pristine $CsPbBr_3$ and four Ni-doped $CsPbBr_3$ 2D NCs using single-color pump (SCP) 800 nm and two-color pump (TCP) 800 + 400 nm utilizing ∼35 fs laser pulses. We firmly believe this is the first report on HHG studies from plasma plumes of $CsPbBr_3$, 0.03% Ni, 0.05% Ni, 0.08% Ni, and 0.1% Ni-doped 2D NCs and correlation of enhancement of the harmonic yield with their third-order NLO coefficients. The exploration of novel and efficient materials (ablated 2D NCs in the present case) in this direction paves ways for proving the leads and means to achieve extreme ultraviolet radiation for a variety of applications in nonlinear spectroscopy and atto-second physics.

2. EXPERIMENTAL DETAILS

2.1. Materials and Methods. Figure 1a,b depicts the schematic of the preparation of pure Cs oleate and Ni-doped $CsPbBr_3$ NCs,

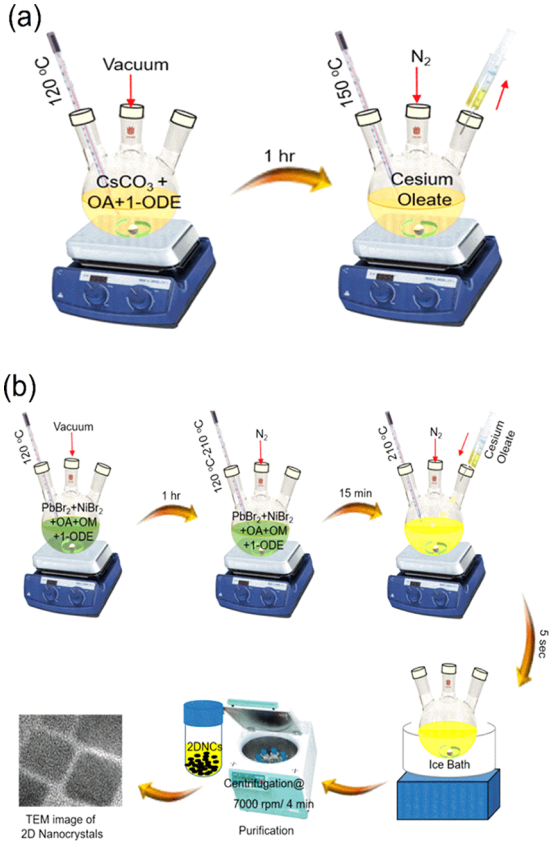

Figure 1. Schematic of the preparation of (a) pure Cs oleate and (b) and Ni-doped $CsPbBr_3$ NCs.

respectively. The complete synthesis procedure and structural characterization (in toluene solvent) of pristine $CsPbBr_3$ and 0.03% Ni-, 0.05% Ni-, 0.08% Ni-, and 0.1% Ni-doped $CsPbBr_3$ were reported in our earlier work.[12]

The synthesized NCs pellets are redispersed in 5 mL of tetrahydrofuran and subjected to transmission electron microscopy (TEM) analysis. Figure 2 illustrates the TEM images of pristine and 0.08% Ni-doped $CsPbBr_3$. The 2D NCs exhibited a square shape with an average particle size of ∼20 nm. The bright lattice fringes of HRTEM images depicted lattice plane distances of 0.394 and 0.390 nm for pristine and Ni-doped $CsPbBr_3$ NCs, respectively. The obtained results are in agreement with the orthorhombic phase of $CsPbBr_3$. The strong, bright diffraction rings in the SAED patterns suggested that the prepared pristine and Ni-doped $CsPbBr_3$ NCs exhibited a well-defined crystalline structure [shown in the insets of Figure 2a,c]. The doping usually influences the size and uniformity of the obtained NCs, and as a consequence, in the case of 0.08% Ni-doped $CsPbBr_3$, a narrow size distribution was achieved.[39]

2.2. High-Order Harmonic Generation Setup. Figure 3 shows the experimental setup for HHG measurements, which consists of a Ti:sapphire laser operating at a wavelength of 800 nm (duration of ∼35 fs) with a repetition rate of 1 kHz. The harmonic spectra were measured using a driving pulse (DP) of 800 nm, 100 Hz (the repetition rate reduced to 100 Hz to see the harmonic spectra without saturation captured by CCD), for pulse duration of 35 fs. Initially, the NCs were in toluene solvent and then these were carefully placed on a glass substrate and left for drying on the substrate (toluene evaporates easily under ambient conditions); the approximated thickness of the NC target was ∼1 mm. Later on, the samples were kept in a target chamber in XYZ stage and ablated by heating pulses (HP) of 200 ps (800 nm, 100 Hz) and 5 ns (1064 nm, 10 Hz, Q-smart 850) to create plasma plumes for HHG measurements. Initially, we had optimized the focusing position of HP, and then after the target was preciously moved along the vertical direction (using the XYZ stage) after measuring HHG spectra, the next set of data, the ablating laser pulse has to expose to a fresh surface without loss of plasma plumes because the already ablated portion leads to a decreased efficiency of creating plasma plumes. The details and description about the HHG experimental setup in terms of DP and HP laser parameters, delays between them, and other optical layouts (lens, mirrors, microchannel plate, gratings, and CCD) used in the present work are already reported in our earlier work.[40]

The reported pristine $CsPbBr_3$ and Ni-doped $CsPbBr_3$ NCs were stable enough during the experiments under laser irradiation in vacuum. For this, we have verified with exposure of UV lamp on the samples before and after measurements of HHG, which shows the emission of efficient photoluminescence. After HHG measurements, the unablated portion of target samples emits bright emission of photoluminescence light, which is comparatively weaker in the ablated area. Moreover, it is important to note that the thickness of the samples does not affect the emission of harmonics and their cutoff. Depending on the intensity of the HP, low-thickness samples will exhaust early and there will be no emission of harmonics. In the case of thick samples for a few shots of ablations, intense harmonics will be obtained, and further ablation on the same position leads to a signal loss because the focus position is changed and the material is already damaged by the intense ablating laser pulse. Therefore, it is necessary to maintain a uniform thickness of the samples for ablation without changing the focus position of the ablating laser pulse.

3. RESULTS AND DISCUSSION

Initially, we compared the harmonic spectra of all samples (refer to $CsPbBr_3$ and four Ni-doped $CsPbBr_3$ 2D NCs) with an SCP and a TCP in the case of ps HP and ns HP at particular intensities of DPs and HPs. In this study, we have chosen a DP duration of 35 fs because in the generation of higher-order harmonics, a shorter pulse duration leads to an increase in the cutoff and intensity of harmonics. Previously, researchers have demonstrated the effect of DP duration on the emission of harmonic for various solid materials, LIPs, and gas jets.[19,41−47] However, in the present report, we have mainly measured harmonics spectra at a 35 fs pulse duration; further, we could not precisely fine-tune the pulse duration in the experiment. Figure 4 illustrates the harmonic spectra obtained from the LIPs of pristine $CsPbBr_3$ and Ni-doped $CsPbBr_3$ (0.1% Ni-doped, 0.08% Ni-doped, 0.05% Ni-doped, and 0.03% Ni-doped) 2D NCs at DP intensity $I_{fs} = 4.5 \times 10^{14}$ W cm^{-2}, and HP intensity $I_{ps} = 1.2 \times 10^{10}$ W cm^{-2}, $I_{ns} = 5.9 \times 10^{10}$ W

https://doi.org/10.1021/acsanm.1c01490
ACS Appl. Nano Mater. 2021, 4, 8292−8301

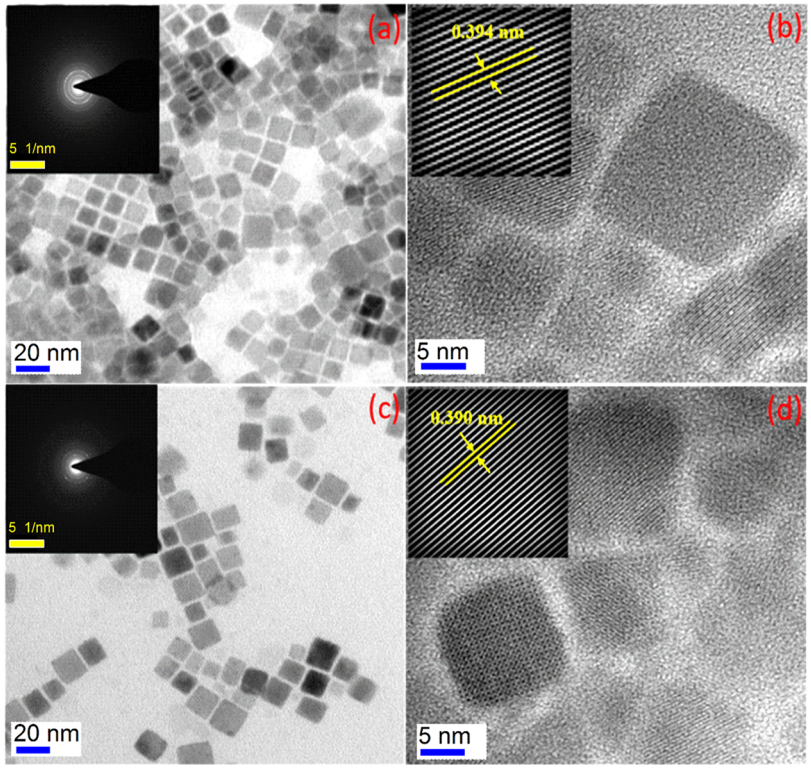

Figure 2. (a) TEM images of pristine $CsPbBr_3$ nanocrystals, with the inset illustrating the SAED pattern. (b) HRTEM image of pristine $CsPbBr_3$ nanocrystals. (c) TEM images of 0.08% Ni-doped $CsPbBr_3$, with the inset illustrating the SAED patterns. (d) HRTEM image of 0.08% Ni-doped $CsPbBr_3$.

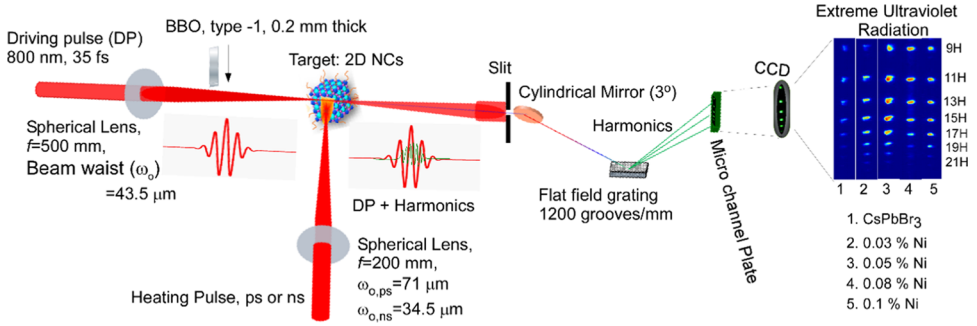

Figure 3. Experimental setup for high-order harmonic generation. Targets: $CsPbBr_3$ and Ni-doped $CsPbBr_3$ 2D NCs. The numbers 1, 2, 3, 4, and 5 correspond to the processed harmonic spectra of $CsPbBr_3$, and 0.03% Ni-, 0.05% Ni-, 0.08% Ni-, and 0.1% Ni-doped $CsPbBr_3$ 2D NCs at $I_{fs} = 2.2 \times 10^{14}$ W cm^{-2} and $I_{ps} = 0.5 \times 10^{10}$ W cm^{-2}. For two-color pump (TCP), we have inserted BBO in the laser propagation direction.

cm^{-2} for (a) SCP, ps HP; (b) SCP, ns HP; (c) TCP, ps HP; and (d) TCP, ns HP. The intensities of harmonics for ps LIP are slightly higher than those for ns LIP for all samples. During the measurement of the cutoff of harmonics, it was observed that for SCP, the harmonic spectra extended up to 27H and 23H for ps LIP, whereas they were limited to 21H and 19H for ns LIP corresponding to Ni-doped $CsPbBr_3$ and $CsPbBr_3$. However, for TCP, Ni-doped $CsPbBr_3$ and $CsPbBr_3$ demonstrated harmonics spectra for ps LIP, which were up to 24H and 16H, whereas for ns LIP, they were 19H and 14H, respectively. The mechanisms of energy absorption, heating, and ablation are significantly affected by the HP duration, which determines the plasma plume characteristics and dynamics. Earlier works have clearly demonstrated that the spatial−temporal distributions of the plasma plumes produced by fs and ns laser pulses are distinctly different from each other.[48−50] For example, Verhoff et al.[48] have recently reported that the angular distribution of ions and evaporated mass was smaller in the case of fs LIP compared to ns LIP. The ns LIP possessed spherical expansion, whereas cylindrical expanded plasmas associated with ps laser pulses exhibited a smaller angular distribution of ions.[40] Additionally, the focal spot size in the case of ps excitation (∼71 μm) was higher than the ns case (34.5 μm) and, therefore, achieved better interaction of DP with ps LIPs. Consequently, this leads to the excitation of a higher density of ions. However, ns LIPs consisted of a greater number of atoms than ions. It is expected that the density of ps LIP is higher and leads to an increased cutoff and harmonic yield compared to ns LIPs, and the supporting data is shown in Figure 4.

In the case of TCP, the results from collinear polarization and orthogonal polarization between fundamental and second harmonics (SH) will be different. In this paper, we only considered the latter case due to the simplicity of the setup.

https://doi.org/10.1021/acsanm.1c01490
ACS Appl. Nano Mater. 2021, 4, 8292−8301

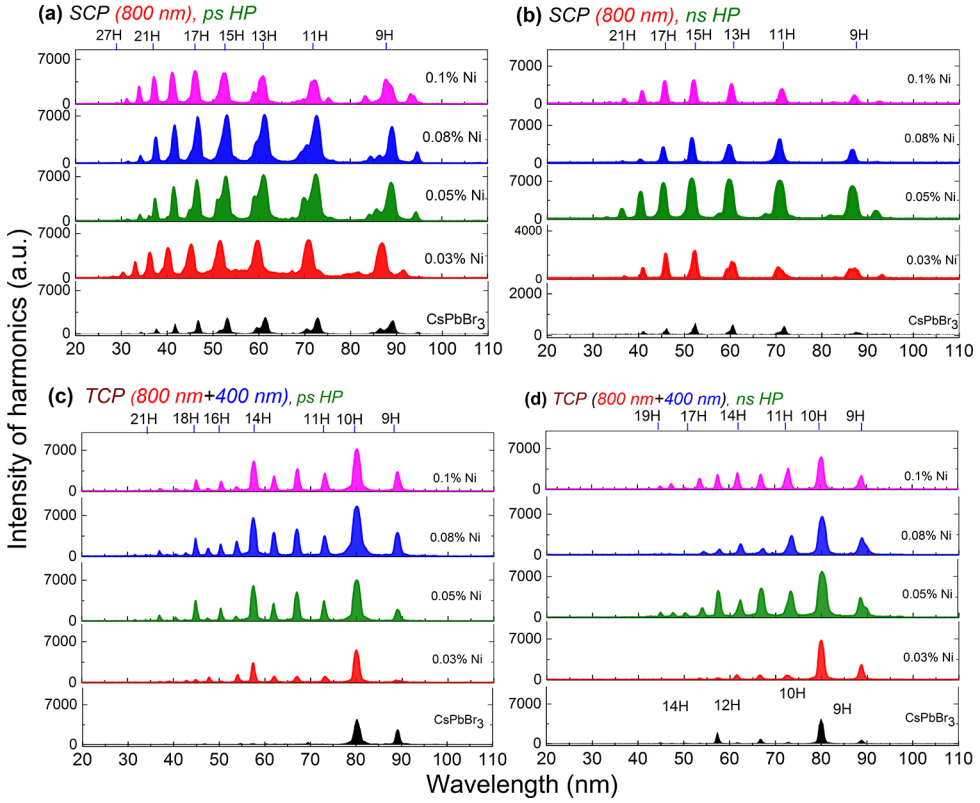

Figure 4. Harmonic spectra measured for all samples using 35 fs pulses: (a) single-color pump, 800 nm, ps heating pulse; (b) SCP, 800 nm, ns HP; (c) two-color pump 800 + 400 nm, ps HP; and (d) TCP, 800 + 400 nm, ns HP at $I_{fs} = 4.5 \times 10^{14}$ W cm^{-2}, and HP for $I_{ps} = 1.2 \times 10^{10}$ W cm^{-2}, $I_{ns} = 5.9 \times 10^{10}$ W cm^{-2}.

We currently do not have the components we need to control the relative phase between 400 and 800 nm. Although we admit that we currently do not have a thorough report with two-color fields, we believe that at least the results demonstrated that both odd and even order harmonics are enhanced due to doping. Previous researchers demonstrated HHG from the plasma plumes of various materials and gas jets using TCP of different wavelengths with orthogonal polarization of SH wavelengths.[51−57] For TCP measurements, a BBO crystal (type 1, 0.2 mm thickness) is placed 20 cm away from the focusing lens providing a SH conversion efficiency of about 20% at $I_{fs} = 4.5 \times 10^{14}$ W cm^{-2}. Therefore, the measured intensity distribution ratio of the fundamental and SH signal was 1.8:1. As per the energy cutoff formula $E_{cut\text{-}off} = I_p + 3.17U_p$ (where I_p is the ionization potential; $U_p = 9.33 \times 10^{-14}/(W/cm^2)\ \lambda^2\ (\mu m)$ is the ponderomotive potential, in which I is the laser intensity at focus, and λ is the wavelength of incident laser pulses), the cutoff of harmonics is proportional to the driving laser wavelength. In the case of TCP, the 400 nm wavelength contributes significantly toward the generation of harmonics with even numbers, whereas SCP generates odd harmonics. Therefore, shorter driving wavelengths lead to decrease in the cutoff of harmonics; as a result, the TCP has lower cutoffs of 24H and 16H than SCP, i.e., 27H and 21H, for Ni-doped $CsPbBr_3$ in the case of ps and ns LIPs, respectively.

It is known that SCP generates only odd harmonics, whereas both odd and even harmonics could be generated with TCP and that too with a higher conversion efficiency. Such an enhancement can be attributed to the selection of a short quantum path component of a denser electron wave packet and a higher ionization rate.[51−53] Overall, Ni-doped $CsPbBr_3$ NCs possessed intense harmonic spectra for TCP compared to SCP. Particularly, in the case of $CsPbBr_3$ for ps HP and ns LIP, the harmonic yield was enhanced by 1.75 and 7 times for TCP than SCP. Meanwhile, in both LIP experiments, the extension of harmonics and higher yield for Ni-doped $CsPbBr_3$ than $CsPbBr_3$ indicates that Ni-dopants play a key role in higher-order harmonics. Among the Ni-doped 2D NCs, there was not a much significant difference in the cutoff, whereas the concentration of Ni-dopants led to an increase in the harmonics yields as illustrated in Figure 4. The maximum harmonic yield for all samples for four different cases is shown in Figure 5b−e. Interestingly, enhancement in the harmonics yield in the case of SCP, ps LIP [shown in Figure 5b] is closely proportional to the third-order NLO properties [nonlinear refractive index (n_2), third-order NLO susceptibility($\chi^{(3)}$)] of the samples measured using the Z-scan technique at 800 nm pulses reported in ref 12, which is shown in Figure 5a. Similarly, this correlation looked very similar to other conditions of DP and HP presented in Figure 5c−e. It describes that for driving pulses of 800 nm (SCP) and a combination of 800 + 400 nm (TCP), the harmonic emission was increased due to the contribution of Ni-dopants in the $CsPbBr_3$ NCs when plasma plumes were obtained with ablation using either ps or ns HPs.

Meanwhile, it is important to have knowledge about the responsible plasma components (atoms, ions, nanoparticles) contributing to the emission of harmonics. During the experiments, by changing HP and DP intensities and the delay between HP and DP (studied the delay dependence with respect to ns HP and fs DP for SCP), we can assume that the probability of species with different masses can contribute to

https://doi.org/10.1021/acsanm.1c01490
ACS Appl. Nano Mater. 2021, 4, 8292−8301

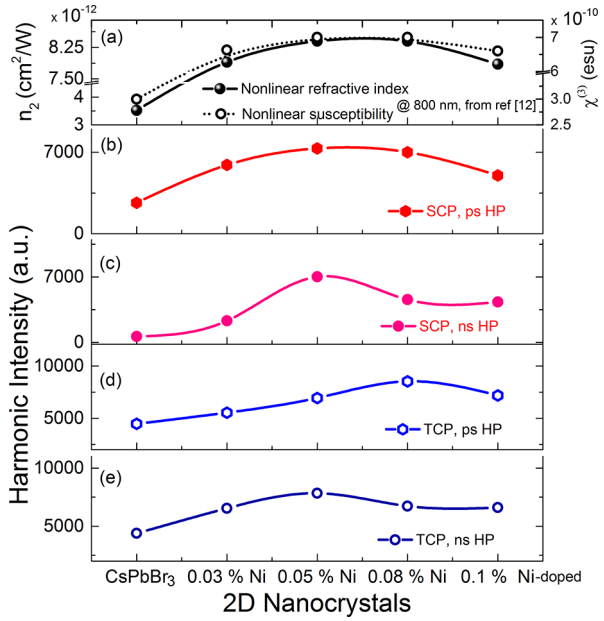

Figure 5. (a) Nonlinear refractive index of the materials taken from ref 12, measured at 800 nm *Z*-scans, and the maximum harmonic yield taken from Figure 3 data for (b) SCP, ps HP; (c) SCP, ns HP; (d) TCP, ps HP; and (e) TCP, ns HP.

HHG. The HHG spectra for different intensities of SCP and ps HP are shown in Figure 6. As expected, the harmonic cutoff and intensity increase with DP and HP intensities. At I_{fs} = 1.2 × 10^{14} W cm^{-2} and I_{ps} = 0.3 × 10^{10} W cm^{-2}, the cutoff was 2 orders higher [21H (Ni-doped) and 17H ($CsPbBr_3$)] and the intensity of harmonics was much stronger for Ni-dopants NCs than the $CsPbBr_3$, as shown in Figure 6a. Consequently, the cutoff appears to be similar (25H) at I_{fs} = 6.0 × 10^{14} W cm^{-2} and I_{ps} = 1.6 × 10^{10} W cm^{-2} for all samples, except for the 0.05% Ni (which has 29H) sample, as shown in the data of Figure 6d. The maximum harmonic yield taken from Figure 6 data for different I_{fs} and I_{ps} is plotted in Figure 7. The

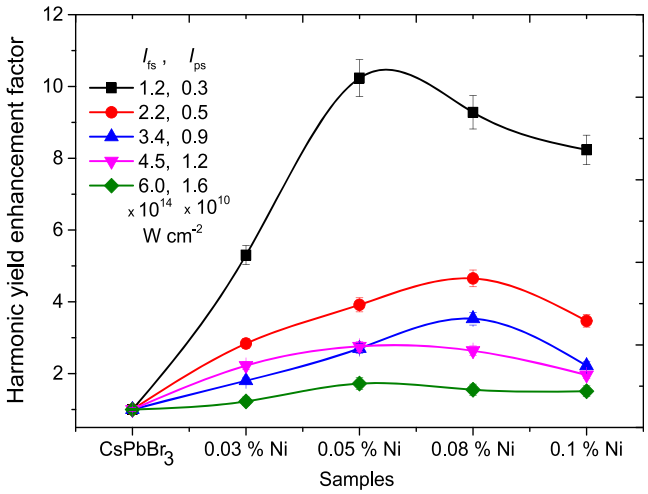

Figure 7. Harmonic yield enhancement factors at various intensities of driving and ps heating pulses.

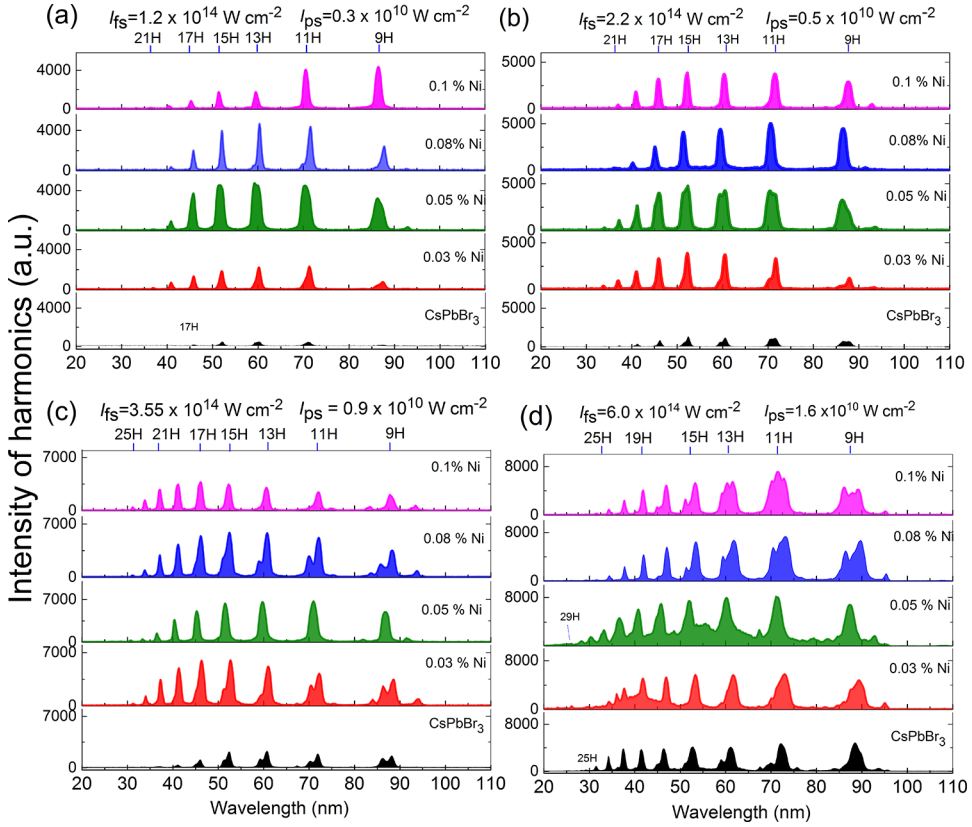

Figure 6. Higher-order harmonic spectra for different intensities of driving and ps heating pulses at (a) I_{fs} = 1.2 × 10^{14} W cm^{-2} and I_{ps} = 0.3 × 10^{10} W cm^{-2}, (b) I_{fs} = 2.2 × 10^{14} W cm^{-2} and I_{ps} = 0.5 × 10^{10} W cm^{-2}, (c) I_{fs} = 3.55 × 10^{14} W cm^{-2} and I_{ps} = 0.9 × 10^{10} W cm^{-2}, and (d) I_{fs} = 6.0 × 10^{14} W cm^{-2} and I_{ps} = 1.6 × 10^{10} W cm^{-2}, respectively.

https://doi.org/10.1021/acsanm.1c01490
ACS Appl. Nano Mater. 2021, 4, 8292−8301

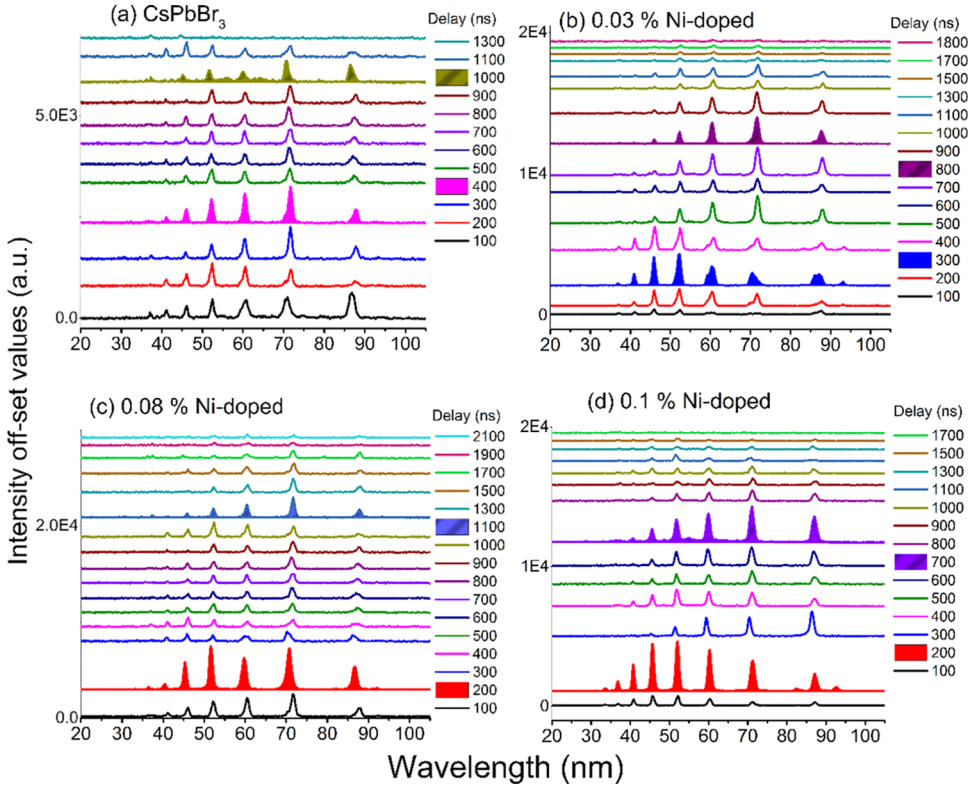

Figure 8. HHG spectra of (a) pristine $CsPbBr_3$, (b) 0.03% Ni, (c) 0.08% Ni, and (d) 0.1% Ni-doped $CsPbBr_3$ 2D nanocrystals for different delay times between nanosecond heating and fs driving pulses.

harmonic yield enhancement factor was found to be significantly higher for lower intensities and was found to be gradually decreasing for higher pulse intensities. This indicates that for the targets ablated with lower I_{ps}, the Ni-dopants considerably contributed to the generation of harmonics, whereas at higher I_{ps} and I_{fs}, the emission of harmonics is significantly contributed by the plasma components of $CsPbBr_3$ (includes Ni components) from all of the samples; as a result, the difference of harmonic yields decreases from pristine $CsPbBr_3$ to Ni-doped $CsPbBr_3$. It is highly likely that at lower DP and HP intensities [shown in Figure 6a,b], the observed harmonic yields are mainly contributed by the neutral atoms rather than the ions of these 2D NCs, which leads to enhancement of the lower-order harmonics (9H to 15H), whereas the contribution of the ions becomes significant at higher DP and HP intensities as shown in Figure 6c,d. In particular, at $I_{fs} = 6.0 \times 10^{14}$ W cm^{-2} and $I_{ps} = 1.6 \times 10^{10}$ W cm^{-2} shown in Figure 6d, the harmonic spectra look saturated possessing a wider full width at half-maximum (FWHM) of each harmonic compared to other intensities of DP and HP.

The plasma plume of the materials ablated in vacuum contains components of the parent material, such as atoms, ions, nanoparticles, and clusters, which could be responsible for HHG. The plasma plume density depends on the ablating laser pulse intensity. However, at the ablating laser pulse intensity of the order of $\sim 10^{10}$, the plasma plumes contain the above-mentioned components. These components play a decisive role in the generation of higher-order harmonics with respect to the DP intensities. The DP intensity decides the cutoff of harmonics as well as the intensity of emitted harmonics due to the dependence of ionization potential and ponderomotive potential of plasma components. Further in situ experimentation is required to identify the exact plasma components responsible for HHG. However, during the experiments, by changing the delay between the ns HP and DP, we can investigate the distribution of substances of different masses in the LIPs of these samples. In this case, the LIPs are generated with the ns HPs where the temporal delay with respect to the DPs could be adjusted electronically using a delay generator, as described in the Experimental Details section. Figure 8 shows the harmonic spectra of $CsPbBr_3$, 0.03% Ni, 0.08% Ni, and 0.1% Ni, and Figure 9a shows the color map of 0.05% Ni-doped $CsPbBr_3$ 2D NCs produced at $I_{fs} = 4.5 \times 10^{14}$ W cm^{-2} and $I_{ns} = 5.9 \times 10^{10}$ W cm^{-2} for several different delays (100−2600 ns range). It is observed that the harmonic yield became weaker with increasing the delay between HP and DP. This could be due to the fact that after certain delays, heavy plasma components are not sufficient enough to generate harmonic signals. However, the harmonic cutoff for each sample was almost insensitive to the delay value. Figure 9b shows the 11H intensity as a function of delay between ns HP and fs DP. In the case of $CsPbBr_3$, up to 1300 ns, the harmonic emission was present, whereas for 0.03% Ni, 0.05% Ni, 0.08% Ni, and 0.01% Ni-doped $CsPbBr_3$ NCs, the delay was extended up to 1800, 2600, 2100, and 1700 ns, respectively [inset of Figure 9b]. It is noteworthy to mention here that the harmonic intensity did not decrease monotonically as a function of delay. It can be seen that there exists a maximum at 200−400 ns (for $CsPbBr_3$, 400 ns; for 0.03% Ni and 0.05% Ni, 300 ns; and for 0.08% Ni and 0.1% Ni, 200 ns). The estimation of the velocity [i.e., distance (0.2 mm)/delay time (ns)] of the main part of emitters equals $(0.5-1.0) \times 10^3$ m/s, which is close to the earlier HHG-based measurements in the case of DP propagation at a 0.2 mm distance from the target surface.[58] More local maxima are at multiples of each 400−600 ns delay difference until their delay cutoff is reached

https://doi.org/10.1021/acsanm.1c01490
ACS Appl. Nano Mater. 2021, 4, 8292−8301

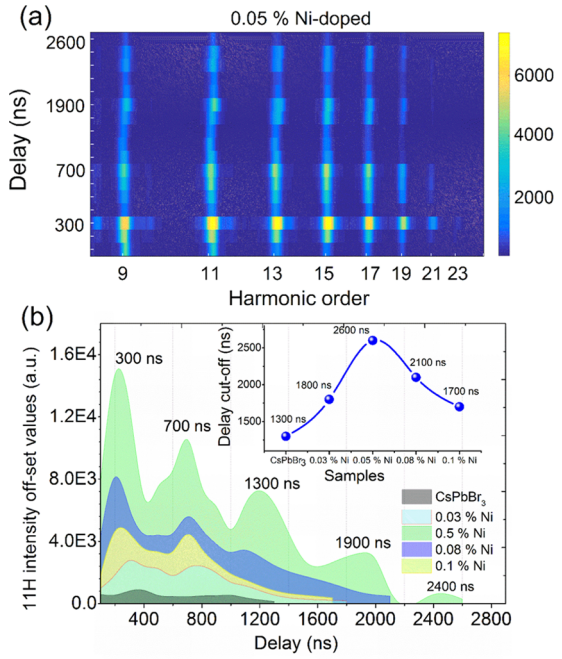

Figure 9. (a) Color map of 0.05% Ni-doped $CsPbBr_3$ NCs at different delays. (b) 11th harmonic intensity for different delays between ns HP and 35 fs DP (800 nm); the inset shows the delay cutoff of all samples.

(for example, we have shown the delay times for 0.05% Ni-doped in Figure 9b). This indicates that the plasma plume consists of similar atoms/ions cluster of these samples having their mass multiple integers of initially coming species (fast components) at similar intensities of DP and ns HP. This also confirms the presence of Ni-dopants, which leads to an increase in the intensity of harmonics at longer delays. For $CsPbBr_3$, we noticed that the delay cutoff was 1300 ns, which includes the second maxima of harmonic intensity near to 1000 ns (has first maxima of harmonics at 400 ns). Here, the difference of the first maximum to the second maximum of harmonic yield was again 600 ns. The DP was propagating ~0.2 mm close to the targets. The calculated velocity of species at 600 ns was 0.33×10^3 m/s yield at these 2D NCs having another maximum intensity approximately after each 400−600 ns delay difference until their delay cutoff was reached. Overall, these delay studies show an indication that the plasma plume consisted of fast and slow components during the laser ablation of ns HP. Also, it was observed that the trend of the delay cutoff curve [inset of Figure 9b] looks similar to the incremental behavior of harmonic intensities and nonlinear refractive index of the reported materials (shown in Figure 5). This indicates that the Ni-dopants enhanced the contribution of harmonic signals at longer delays. These studies clearly demonstrate that Ni-dopant NCs had maximum harmonic spectra at lower delays than $CsPbBr_3$, which implies that Ni-dopant NCs consisted of faster components than $CsPbBr_3$.

Overall, the HHG measurements reported in this work indicate that pristine ($CsPbBr_3$) possesses intense harmonics; however, Ni-dopants increased the enhancement of the harmonic yield. The third-order NLO properties of pristine $CsPbBr_3$ and Ni-doped $CsPbBr_3$ 2D NCs were investigated earlier by Ketavath et al. using the fs Z-scan technique.[12] Strong 2PA coefficients and third-order NLO susceptibility values were obtained for Ni-doped $CsPbBr_3$. The enhanced NLO properties might be attributed to the localized surface plasmon-induced charge transfer. However, in the present report, we have measured the higher-order harmonics from LIPs of the reported 2D NCs. It is well known that HHG is a three-step model[59] involving the following steps: (a) ionization by the strong field associated with focused input laser pulses, (b) acceleration of particles in the laser field, and (iii) recombination with the parent ion followed by emission of a high-energy photon. Further, the emission of harmonics significantly depends on the density of plasma components such as the parent molecule's atoms, ions, and nanoparticles. The emitted harmonics (XUV radiation) are highly coherent with fundamental beams, which are the resultant of individual harmonics emitted by each component in the plasma plumes. Here, the first and second ionization potentials of Cs, Pb, Br and Ni are given by 3.894, 7.416, 11.814, and 7.6398 and 23.15745, 15.0322, 21.8, and 18.16884 eV, respectively. The supplied DP intensity is enough to iterate the harmonics from either atoms or ions or both. As discussed above, the Ni-doped NCs contain additional Ni atoms or ions in their plasma components compared to the undoped/pure $CsPbBr_3$ NCs. Therefore, it is expected that the plasma density of Ni-doped $CsPbBr_3$ NCs is higher than the undoped $CsPbBr_3$ NCs and, as a result, high intense harmonics are emitted. However, it is assumed that other dopants to $CsPbBr_3$ NCs or other perovskites might lead to an increase in the emission of higher-order harmonics due to an increase of their plasma density during laser ablation of respective targets. For instance, Zhou et al. reported the controlled doping of monovalent Ag^+ into $CsPbBr_3$ NCs via a simple room-temperature synthesis procedure and explored the electrical properties of halide perovskite NCs,[60] and other research groups have successfully synthesized different perovskites with Ag-doping.[61−63] It is expected that these Ag-doped perovskite NCs or thin films will be useful for emission intense higher-order harmonics because Ag is one of the promising materials that itself emits stronger and higher cutoff of harmonics from its LIPs.[40,64,65] Thus, the present study opens an entirely new approach for researchers to synthesize stable new perovskite NCs with other dopants, which are helpful toward the emission of intense harmonics from their laser-induced plasmas.

4. CONCLUSIONS

In summary, we have presented results from our detailed studies on the HHG in the plasmas generated from five 2D NCs (pristine $CsPbBr_3$, four Ni-doped CsPbBr3 with 0.03% Ni, 0.05% Ni, 0.08% Ni and 0.1% Ni, respectively). The contribution of Ni-dopants in laser-ablated plume (ablated by ps HP and ns HP) from 2D NCs has been analyzed for both SCP and TCP driving pulses. The measurements were performed at different intensities of SCP, and we have also demonstrated the difference of delay dependence curves between $CsPbBr_3$ and Ni-doped $CsPbBr_3$ containing 2D NCs while recognizing the similarity of the optimal values of delays for different species at which the highest harmonic yield was achieved. By combining the analysis of delay dependences of integrated harmonics signals and HHG spectra in the 20−100 nm wavelength range, the role of Ni-dopants, small- and large-sized 2D NCs in the former process have been revealed. We have established that the presence of Ni-dopants and combined 2D NCs fragments leads to an enhancement in harmonics signal in the wavelength range of 35−90 nm (i.e., harmonics from 9H to 25H orders), especially in Ni-doped

https://doi.org/10.1021/acsanm.1c01490
ACS Appl. Nano Mater. 2021, 4, 8292−8301

NCs. The 2D NCs species possess better enhancement of harmonics yield at lower DP and HP intensities. The important role of utilizing two DP (i.e., SCP and TCP) and two HP (i.e., picosecond and nanosecond) laser pulses is that we can digitally control extensive delays between heating and driving pulses. The present studies allowed a better understanding of the enhancement of plasma spreading dynamics in the harmonics generation from ablated species comprising similar Ni-dopants with a variable concentration. In the case of $CsPbBr_3$, the first maximum was achieved at 400 ns, and it decreased to 300 ns (0.03% Ni, 0.05% Ni) and 200 ns (0.08% Ni and 0.1% Ni), which illustrates that a higher concentration of Ni emits first set of fast components. However, other maximum intensities were achieved approximately after each 400−600 ns delay difference until their delay cutoff was reached. Our detailed results and observations have demonstrated that under optimal ablation conditions, the laser-produced plasmas on surfaces of different Ni-doped and pure $CsPbBr_3$ 2D NCs contained species spread out with comparable velocities. We analyzed the HHG yield for four different cases; the enhancement of harmonics yields in the case of SCP, ps LIP was exactly comparative to the third-order NLO properties (nonlinear refractive index and NLO susceptibility) of the samples. Similarly, this correlation was similar to SCP (ns HP), TCP (ps and ns HP), and the extension of delay pattern for these five samples. The emission of harmonics from LIP of pristine, Ni-doped $CsPbBr_3$ NCs reported here supposedly provide the means to address the optimization of extreme ultraviolet radiation arising from structural differences. Also, the exploration of novel and efficient materials in HHG direction paves ways to achieve extreme ultraviolet radiation for a variety of applications in nonlinear spectroscopy and attosecond physics.

AUTHOR INFORMATION

Corresponding Authors

Srinivasa Rao Konda − *GPL, State Key Laboratory of Applied Optics, Changchun Institute of Optics, Fine Mechanics and Physics, Chinese Academy of Sciences, Changchun 130033, China;* orcid.org/0000-0002-9001-4857; Email: ksrao@ciomp.ac.cn

Wei Li − *GPL, State Key Laboratory of Applied Optics, Changchun Institute of Optics, Fine Mechanics and Physics, Chinese Academy of Sciences, Changchun 130033, China; University of Chinese Academy of Sciences, Beijing 100049, China*; Email: weili1@ciomp.ac.cn

Authors

Venugopal Rao Soma − *Advanced Center of Research in High Energy Materials (ACRHEM), University of Hyderabad, Hyderabad 500046 Telangana, India*

Murali Banavoth − *Solar Cells and Photonics Research Laboratory, School of Chemistry, University of Hyderabad, Hyderabad 500046 Telangana, India*

Ravi Ketavath − *Solar Cells and Photonics Research Laboratory, School of Chemistry, University of Hyderabad, Hyderabad 500046 Telangana, India*

Venkatesh Mottamchetty − *GPL, State Key Laboratory of Applied Optics, Changchun Institute of Optics, Fine Mechanics and Physics, Chinese Academy of Sciences, Changchun 130033, China*

Yu Hang Lai − *GPL, State Key Laboratory of Applied Optics, Changchun Institute of Optics, Fine Mechanics and Physics, Chinese Academy of Sciences, Changchun 130033, China; University of Chinese Academy of Sciences, Beijing 100049, China*

Complete contact information is available at: https://pubs.acs.org/10.1021/acsanm.1c01490

Author Contributions

S.R.K. contributed to conceptualization, data acquisition, investigation, methodology, writing the original draft, and review and editing. V.R.S. involved in conceptualization and review and editing. M.B. and R.K. performed synthesis and characterization. V.M. contributed to data acquisition. Y.H.L. involved in conceptualization and review and editing. W.L. contributed to supervision, review and editing, funding acquisition, and project administration.

Notes

The authors declare no competing financial interest.

ACKNOWLEDGMENTS

Srinivasa Rao Konda acknowledges support by the Chinese Academy of Sciences President's International Fellowship Initiative [grant no. 2021PM0036]. This work was supported by The Innovation Grant of Changchun Institute of Optics, Fine Mechanics and Physics (CIOMP), Development Program of the Science and Technology of Jilin Province, 20200802001GH,National Natural Science Foundation of China [grant no. 12004380], Jilin Provincial Science & Technology Development Project [grant no. YDZJ202102CXJD002], and the K. C. Wong Education Foundation (grant no. GJTD-2018−08). Venugopal Rao Soma acknowledges DRDO, India, for financial support through the project ERIP/ER/1501138/M/01/319/D(R&D).

ABBREVIATIONS

2D, two-dimensional
2PA, two-photon absorption
DP, driving pulse
HP, heating pulse
HHG, high-order harmonic generation
LIP, laser-induced plasma
NCs, nanocrystals
NLO, nonlinear optical
SCP, single-color pump
SH, second harmonic
TCP, two-color pump
TEM, transmission electron microscopy
XUV, extreme ultraviolet

REFERENCES

(1) Xu, Y.; Chen, Q.; Zhang, C.; Wang, R.; Wu, H.; Zhang, X.; Xing, G.; Yu, W. W.; Wang, X.; Zhang, Y.; Xiao, M. Two-Photon-Pumped Perovskite Semiconductor Nanocrystal Lasers. *J. Am. Chem. Soc.* **2016**, *138*, 3761−3768.

(2) Li, P.; Chen, Y.; Yang, T.; Wang, Z.; Lin, H.; Xu, Y.; Li, L.; Mu, H.; Shivananju, B. N.; Zhang, Y.; Zhang, Q.; Pan, A.; Li, S.; Tang, D.; Jia, B.; Zhang, H.; Bao, Q. Two-Dimensional $CH_3NH_3PbI_3$ Perovskite Nanosheets for Ultrafast Pulsed Fiber Lasers. *ACS Appl. Mater. Interfaces* **2017**, *9*, 12759−12765.

(3) Zhu, H.; Fu, Y.; Meng, F.; Wu, X.; Gong, Z.; Ding, Q.; Gustafsson, M. V.; Trinh, M. T.; Jin, S.; Zhu, X. Y. Lead Halide Perovskite Nanowire Lasers with Low Lasing Thresholds and High Quality Factors. *Nat. Mater.* **2015**, *14*, 636−642.

(4) Xing, G.; Mathews, N.; Lim, S. S.; Yantara, N.; Liu, X.; Sabba, D.; Grätzel, M.; Mhaisalkar, S.; Sum, T. C. Low-Temperature Solution-Processed Wavelength-Tunable Perovskites for Lasing. *Nat. Mater.* **2014**, *13*, 476−480.
(5) Kanemitsu, Y.; Handa, T. Photophysics of Metal Halide Perovskites: From Materials to Devices. *Jpn. J. Appl. Phys.* **2018**, *57*, No. 090101.
(6) Hoye, R. L. Z.; Lai, M. L.; Anaya, M.; Tong, Y.; Gałkowski, K.; Doherty, T.; Li, W.; Huq, T. N.; Mackowski, S.; Polavarapu, L.; Feldmann, J.; Macmanus-Driscoll, J. L.; Friend, R. H.; Urban, A. S.; Stranks, S. D. Identifying and Reducing Interfacial Losses to Enhance Color-Pure Electroluminescence in Blue-Emitting Perovskite Nanoplatelet Light-Emitting Diodes. *ACS Energy Lett.* **2019**, *4*, 1181−1188.
(7) Sadhanala, A.; Ahmad, S.; Zhao, B.; Giesbrecht, N.; Pearce, P. M.; Deschler, F.; Hoye, R. L. Z.; Gödel, K. C.; Bein, T.; Docampo, P.; Dutton, S. E.; De Volder, M. F. L.; Friend, R. H. Blue-Green Color Tunable Solution Processable Organolead Chloride-Bromide Mixed Halide Perovskites for Optoelectronic Applications. *Nano Lett.* **2015**, *15*, 6095−6101.
(8) Chen, Z.; Segev, M. Highlighting Photonics: Looking into the next Decade. *eLight* **2021**, *1*, 1−12.
(9) Zhang, R.; Fan, J.; Zhang, X.; Yu, H.; Zhang, H.; Mai, Y.; Xu, T.; Wang, J.; Snaith, H. J. Nonlinear Optical Response of Organic−Inorganic Halide Perovskites. *ACS Photonics* **2016**, *3*, 371−377.
(10) Yamada, Y.; Yamada, T.; Phuong, L. Q.; Maruyama, N.; Nishimura, H.; Wakamiya, A.; Murata, Y.; Kanemitsu, Y. Dynamic Optical Properties of $CH_3NH_3PbI_3$ Single Crystals As Revealed by One- and Two-Photon Excited Photoluminescence Measurements. *J. Am. Chem. Soc.* **2015**, *137*, 10456−10459.
(11) Li, P.; Chen, Y.; Yang, T.; Wang, Z.; Lin, H.; Xu, Y.; Li, L.; Mu, H.; Shivananju, B. N.; Zhang, Y.; Zhang, Q.; Pan, A.; Li, S.; Tang, D.; Jia, B.; Zhang, H.; Bao, Q. Two-Dimensional $CH_3NH_3PbI_3$ Perovskite Nanosheets for Ultrafast Pulsed Fiber Lasers. *ACS Appl. Mater. Interfaces* **2017**, *9*, 12759−12765.
(12) Ketavath, R.; Katturi, N. K.; Ghugal, S. G.; Kolli, H. K.; Swetha, T.; Soma, V. R.; Murali, B. Deciphering the Ultrafast Nonlinear Optical Properties and Dynamics of Pristine and Ni-Doped $CsPbBr_3$ Colloidal Two-Dimensional Nanocrystals. *J. Phys. Chem. Lett.* **2019**, *10*, 5577−5584.
(13) Zhang, F.; Zhong, H.; Chen, C.; Wu, X. G.; Hu, X.; Huang, H.; Han, J.; Zou, B.; Dong, Y. Brightly Luminescent and Color-Tunable Colloidal $CH_3NH_3PbX_3$ (X = Br, I, Cl) Quantum Dots: Potential Alternatives for Display Technology. *ACS Nano* **2015**, *9*, 4533−4542.
(14) Protesescu, L.; Yakunin, S.; Bodnarchuk, M. I.; Krieg, F.; Caputo, R.; Hendon, C. H.; Yang, R. X.; Walsh, A.; Kovalenko, M. V. Nanocrystals of Cesium Lead Halide Perovskites ($CsPbX_3$, X = Cl, Br, and I): Novel Optoelectronic Materials Showing Bright Emission with Wide Color Gamut. *Nano Lett.* **2015**, *15*, 3692−3696.
(15) Rana, P. J. S.; Swetha, T.; Mandal, H.; Saeki, A.; Bangal, P. R.; Singh, S. P. Energy Transfer Dynamics of Highly Stable Fe^{3+} Doped $CsPbCl_3$ Perovskite Nanocrystals with Dual-Color Emission. *J. Phys. Chem. C* **2019**, *123*, 17026−17034.
(16) Lu, C. H.; Biesold-Mcgee, G. V.; Liu, Y.; Kang, Z.; Lin, Z. Doping and Ion Substitution in Colloidal Metal Halide Perovskite Nanocrystals. *Chem. Soc. Rev.* **2020**, *49*, 4953−5007.
(17) Sanari, Y.; Hirori, H.; Aharen, T.; Tahara, H.; Shinohara, Y.; Ishikawa, K. L.; Otobe, T.; Xia, P.; Ishii, N.; Itatani, J.; Sato, S. A. Role of Virtual Band Population for High Harmonic Generation in Solids. *Phys. Rev. B* **2020**, *102*, No. 041125.
(18) Chang, Z.; Corkum, P. Attosecond Photon Sources: The First Decade and beyond [Invited]. *J. Opt. Soc. Am. B* **2010**, *27*, B9−17.
(19) Feng, X.; Gilbertson, S.; Mashiko, H.; Wang, H.; Khan, S. D.; Chini, M.; Wu, Y.; Zhao, K.; Chang, Z. Generation of Isolated Attosecond Pulses with 20 to 28 Femtosecond Lasers. *Phys. Rev. Lett.* **2009**, *103*, No. 183901.
(20) Li, Z.; Brown, G.; Ko, D. H.; Kong, F.; Arissian, L.; Corkum, P. B. Perturbative High Harmonic Wave Front Control. *Phys. Rev. Lett.* **2017**, *118*, No. 033905.
(21) Kong, F.; Zhang, C.; Bouchard, F.; Li, Z.; Brown, G. G.; Ko, D. H.; Hammond, T. J.; Arissian, L.; Boyd, R. W.; Karimi, E.; Corkum, P. B. Controlling the Orbital Angular Momentum of High Harmonic Vortices. *Nat. Commun.* **2017**, *8*, No. 14970.
(22) Fareed, M. A.; Strelkov, V. V.; Thire, N.; Mondal, S.; Schmidt, B. E.; Legare, F.; Ozaki1, T. High-Order Harmonic Generation from the Dressed Autoionizing States. *Nat. Commun.* **2017**, *8*, No. 16061.
(23) Elouga Bom, L. B.; Haessler, S.; Gobert, O.; Perdrix, M.; Lepetit, F.; Hergott, J.-F.; Carré, B.; Ozaki, T.; Salières, P. Attosecond Emission from Chromium Plasma. *Opt. Express* **2011**, *19*, 3677−3685.
(24) Pertot, Y.; Chen, S.; Khan, S. D.; Bom, L. B. E.; Ozaki, T.; Chang, Z. Generation of Continuum High-Order Harmonics from Carbon Plasma Using. *J. Phys. B: At., Mol. Opt. Phys.* **2012**, *45*, No. 074017.
(25) Rosenthal, N.; Marcus, G. Discriminating between the Role of Phase Matching and That of the Single-Atom Response in Resonance Plasma-Plume High-Order Harmonic Generation. *Phys. Rev. Lett.* **2015**, *115*, No. 133901.
(26) Li, J.; Lu, J.; Chew, A.; Han, S.; Li, J.; Wu, Y.; Wang, H.; Ghimire, S.; Chang, Z. Attosecond Science Based on High Harmonic Generation from Gases and Solids. *Nat. Commun.* **2020**, *11*, No. 2748.
(27) Popmintchev, T.; Chen, M.-C.; Arpin, P.; Murnane, M. M.; Kapteyn, H. C. The Attosecond Nonlinear Optics of Bright Coherent X-Ray Generation. *Nat. Photonics* **2010**, *4*, 822−832.
(28) Ndabashimiye, G.; Ghimire, S.; Wu, M.; Browne, D. A.; Schafer, K. J.; Gaarde, M. B.; Reis, D. A. Solid-State Harmonics beyond the Atomic Limit. *Nature* **2016**, *534*, 520−523.
(29) Hohenleutner, M.; Langer, F.; Schubert, O.; Knorr, M.; Huttner, U.; Koch, S. W.; Kira, M.; Huber, R. Real-Time Observation of Interfering Crystal Electrons in High-Harmonic Generation. *Nature* **2015**, *523*, 572−575.
(30) Ghimire, S.; Dichiara, A. D.; Sistrunk, E.; Agostini, P.; Dimauro, L. F.; Reis, D. A. Observation of High-Order Harmonic Generation in a Bulk Crystal. *Nat. Phys.* **2011**, *7*, 138−141.
(31) Vampa, G.; Hammond, T. J.; Thiré, N.; Schmidt, B. E.; Légaré, F.; McDonald, C. R.; Brabec, T.; Corkum, P. B. Linking High Harmonics from Gases and Solids. *Nature* **2015**, *522*, 462−464.
(32) Schubert, O.; Hohenleutner, M.; Langer, F.; Urbanek, B.; Lange, C.; Huttner, U.; Golde, D.; Meier, T.; Kira, M.; Koch, S. W.; Huber, R. Sub-Cycle Control of Terahertz High-Harmonic Generation by Dynamical Bloch Oscillations. *Nat. Photonics* **2014**, *8*, 119−123.
(33) Ganeev, R. A.; Suzuki, M.; Baba, M.; Ichihara, M.; Kuroda, H. Low- and High-Order Nonlinear Optical Properties of Au, Pt, Pd, and Ru Nanoparticles. *J. Appl. Phys.* **2008**, *103*, No. 063102.
(34) Singhal, H.; Naik, P. A.; Kumar, M.; Chakera, J. A.; Gupta, P. D. Enhanced Coherent Extreme Ultraviolet Emission through High Order Harmonic Generation from Plasma Plumes Containing Nanoparticles. *J. Appl. Phys.* **2014**, *115*, No. 033104.
(35) Ganeev, R. A. Harmonic Generation from Partially Ionized Plasma [Invited]. *J. Opt. Soc. Am. B* **2014**, *31*, 2221−2231.
(36) Fu, Y.; Ganeev, R. A.; Boltaev, G. S.; Maurya, S. K.; Kim, V. V.; Zhao, C.; Rout, A.; Guo, C. Low- and High-Order Nonlinear Optical Properties of Ag_2S Quantum Dot Thin Films. *Nanophotonics* **2019**, *8*, 849−858.
(37) Hirori, H.; Xia, P.; Shinohara, Y.; Otobe, T.; Sanari, Y.; Tahara, H.; Ishii, N.; Itatani, J.; Ishikawa, K. L.; Aharen, T.; Ozaki, M.; Wakamiya, A.; Kanemitsu, Y. High-Order Harmonic Generation from Hybrid Organic-Inorganic Perovskite Thin Films. *APL Mater.* **2019**, *7*, No. 041107.
(38) Nakagawa, K.; Hirori, H.; Sanari, Y.; Sekiguchi, F.; Sato, R.; Saruyama, M. Interference Effects in High-Order Harmonics from Colloidal Perovskite Nanocrystals Excited by an Elliptically Polarized Laser. *Phys. Rev. Mater.* **2021**, *5*, No. 016001.
(39) Yong, Z. J.; Guo, S. Q.; Ma, J. P.; Zhang, J. Y.; Li, Z. Y.; Chen, Y. M.; Zhang, B.; Zhou, Y.; Shu, J.; Gu, J. L.; Zheng, L. R.; Bakr, O. M.; Sun, H. T. Doping-Enhanced Short-Range Order of Perovskite Nanocrystals for Near-Unity Violet Luminescence Quantum Yield. *J. Am. Chem. Soc.* **2018**, *140*, 9942−9951.

https://doi.org/10.1021/acsanm.1c01490
ACS Appl. Nano Mater. 2021, 4, 8292−8301

(40) Srinivasa Rao, K.; Lai, Y. H.; Li, W. Investigation of High Harmonic Generation from Laser Ablated Plumes of Silver. *J. Appl. Phys.* **2021**, *130*, No. 013101.
(41) Légaré, K.; Safaei, R.; Barrette, G.; Arias, L.; Lassonde, P.; Ibrahim, H.; Vodungbo, B.; Jal, E.; Lüning, J.; Jaouen, N.; Tao, Z.; Baltuška, A.; Légaré, F.; Fan, G. K. Raman Red-Shift Compressor: A Simple Approach for Scaling the High Harmonic Generation Cut-Off. *J. Med. Virol.* **2020**, No. 2100113.
(42) Lee, D. G.; Kim, J. H.; Hong, K. H.; Nam, C. H. Coherent Control of High-Order Harmonics with Chirped Femtosecond Laser Pulses. *Phys. Rev. Lett.* **2001**, *87*, No. 243902.
(43) Tosa, V.; Kim, H. T.; Kim, I. J.; Nam, C. H. High-Order Harmonic Generation by Chirped and Self-Guided Femtosecond Laser Pulses. I. Spatial and Spectral Analysis. *Phys. Rev. A* **2005**, *71*, No. 063807.
(44) Han, J.-X.; Wang, J.; Qiao, Y.; Liu, A.-H.; Guo, F.-M.; Yang, Y.-J. Significantly Enhanced Conversion Efficiency of High-Order Harmonic Generation by Introducing Chirped Laser Pulses into Scheme of Spatially Inhomogeneous Field. *Opt. Express* **2019**, *27*, 8768.
(45) Fan, J. G.; Miao, X. Y.; Jia, X. F. Control of the High-Order Harmonic Generation by Sculpting Waveforms with Chirp in Solids. *Chem. Phys. Lett.* **2021**, *762*, No. 138136.
(46) Neyra, E.; Videla, F.; Pérez-Hernández, J. A.; Ciappina, M. F.; Roso, L.; Torchia, G. A. High-Order Harmonic Generation Driven by Chirped Laser Pulses Induced by Linear and Non Linear Phenomena. *Eur. Phys. J. D* **2016**, *70*, No. 243.
(47) Yun, C. X.; Teng, H.; Zhang, W.; Zhan, M. J.; Han, H. N.; Zhong, X.; Wei, Z. Y.; Wang, B. B.; Hou, X. High-Order Harmonics Generation by Few-Cycle and Multi-Cycle Femtosecond Laser Pulses. *Chin. Phys. B* **2010**, *19*, No. 124210.
(48) Verhoff, B.; Harilal, S. S.; Freeman, J. R.; Diwakar, P. K.; Hassanein, A. Dynamics of Femto- and Nanosecond Laser Ablation Plumes Investigated Using Optical Emission Spectroscopy. *J. Appl. Phys.* **2012**, *112*, No. 093303.
(49) Mao, S. S.; Mao, X.; Greif, R.; Russo, R. E. Initiation of an Early-Stage Plasma during Picosecond Laser Ablation of Solids. *Appl. Phys. Lett.* **2000**, *77*, 2464−2466.
(50) Gurlui, S.; Agop, M.; Nica, P.; Ziskind, M.; Focsa, C. Experimental and Theoretical Investigations of a Laser-Produced Aluminum Plasma. *Phys. Rev. E* **2008**, *78*, No. 026405.
(51) Kim, I. J.; Kim, C. M.; Kim, H. T.; Lee, G. H.; Lee, Y. S.; Park, J. Y.; Cho, D. J.; Nam, C. H. Highly Efficient High-Harmonic Generation in an Orthogonally Polarized Two-Color Laser Field. *Phys. Rev. Lett.* **2005**, *94*, No. 243901.
(52) Boltaev, G. S.; Iqbal, M.; Abbasi, N. A.; Kim, V. V.; Ganeev, R. A.; Alnaser, A. S. Enhanced XUV Harmonics Generation from Diatomic Gases Using Two Orthogonally Polarized Laser Fields. *Sci. Rep.* **2021**, *11*, No. 5534.
(53) Ganeev, R. A.; Kuroda, H. High-Order Harmonics Generation in Atomic and Molecular Zinc Plasmas. *Photonics* **2021**, *8*, 29.
(54) Liang, J.; Venkatesh, M.; Boltaev, G. S.; Ganeev, R. A.; Lai, Y. H.; Guo, C. Investigation of Resonance-Enhanced High-Order Harmonics by Two-Component Laser-Produced Plasmas. *Atoms* **2021**, *9*, 1−6.
(55) Ganeev, R. A.; Strelkov, V. V.; Hutchison, C.; Zaïr, A.; Kilbane, D.; Khokhlova, M. A.; Marangos, J. P. Experimental and Theoretical Studies of Two-Color-Pump Resonance-Induced Enhancement of Odd and Even Harmonics from a Tin Plasma. *Phys. Rev. A* **2012**, *85*, No. 023832.
(56) Ganeev, R. A.; Singhal, H.; Naik, P. A.; Chakera, J. A.; Vora, H. S.; Khan, R. A.; Gupta, P. D. Systematic Studies of Two-Color Pump-Induced High-Order Harmonic Generation in Plasma Plumes. *Phys. Rev. A* **2010**, *82*, 053831.
(57) Ganeev, R. A.; Boltaev, G. S.; Stremoukhov, S. Y.; Kim, V. V.; Andreev, A. V.; Alnaser, A. S. High-Order Harmonic Generation during Different Overlaps of Two-Colored Pulses in Laser-Produced Plasmas and Gases. *Eur. Phys. J. D* **2020**, *74*, No. 199.
(58) Ganeev, R. A.; Kim, V. V.; Rao, K. S.; Guo, C. Probing Laser Plasma Dynamics Using High-Order Harmonics Generation in Carbon-Containing Nanomaterials. *Appl. Sci.* **2021**, *11*, No. 2143.
(59) Balcou, P.; Ivanov, M. Y.; Huillier, A. L.; Corkum, P. B. Theory of High-Harmonic Generation by Low-Frequency Laser Fields. *Phys. Rev. A* **1994**, *49*, No. 2117.
(60) Zhou, S.; Ma, Y.; Zhou, G.; Xu, X.; Qin, M.; Li, Y.; Hsu, Y. J.; Hu, H.; Li, G.; Zhao, N.; Xu, J.; Lu, X. Ag-Doped Halide Perovskite Nanocrystals for Tunable Band Structure and Efficient Charge Transport. *ACS Energy Lett.* **2019**, *4*, 534−541.
(61) Kang, M. S.; Sahu, A.; Frisbie, C. D.; Norris, D. J. Influence of Silver Doping on Electron Transport in Thin Films of PbSe Nanocrystals. *Adv. Mater.* **2013**, *25*, 725−731.
(62) Huang, X.; Li, H.; Zhang, C.; Tan, S.; Chen, Z.; Chen, L.; Lu, Z.; Wang, X.; Xiao, M. Efficient Plasmon-Hot Electron Conversion in Ag-$CsPbBr_3$ Hybrid Nanocrystals. *Nat. Commun.* **2019**, *10*, No. 1163.
(63) Chen, Q.; Chen, L.; Ye, F.; Zhao, T.; Tang, F.; Rajagopal, A.; Jiang, Z.; Jiang, S.; Jen, A. K. Y.; Xie, Y.; Cai, J.; Chen, L. Ag-Incorporated Organic-Inorganic Perovskite Films and Planar Heterojunction Solar Cells. *Nano Lett.* **2017**, *17*, 3231−3237.
(64) Ganeev, R. A.; Baba, M.; Suzuki, M.; Kuroda, H. High-Order Harmonic Generation from Silver Plasma. *Phys. Lett. A* **2005**, *339*, 103−109.
(65) Ganeev, R. A.; Suzuki, M.; Baba, M.; Ichihara, M.; Kuroda, H. High-Order Harmonic Generation in Ag Nanoparticle-Containing Plasma. *J. Phys. B: At., Mol. Opt. Phys.* **2008**, *41*, No. 045603.

https://doi.org/10.1021/acsanm.1c01490
ACS Appl. Nano Mater. 2021, 4, 8292−8301